EQCM for In-depth Study of Metal Anodes for Electrochemical Energy Storage①

QIN Run-Zhi WANG Yan ZHAO Qing-He
YANG Kai PAN Feng②
(*School of Advanced Materials, Peking University, Shenzhen Graduate School, Shenzhen* 518055*, China*)

ABSTRACT Electrochemical quartz crystal microbalance (EQCM) is a powerful tool to study the mass change and charge transfer during electrochemical process. The mass change on the electrode surface can be monitored with high precision and high sensitivity, making it possible to analyze the in-depth mechanism of electrode reactions. The application of metal anodes has exhibited great potential for the future energy storage devices for the elevated capacity. Herein, we review the research progress utilizing EQCM for metal anodes, including the deposition/dissolution process, the side reactions, the effect of additives, etc. Furthermore, we also put forward a perspective on research of the mechanism and performance improvement of metal anodes.

Keywords: EQCM, lithium, zinc, anode reaction, energy storage;
DOI: 10.14102/j.cnki.0254–5861.2011–2819

1 INTRODUCTION

Electrochemical quartz crystal microbalance (EQCM) is a gravimetric analysis tool based on the piezoelectric effect of quartz crystal. A shear wave is generated across the thickness of the crystal when it is electrically vibrated into resonance. The dependence of mass change and resonance frequency change of the quartz electrode can be estimated by the Sauerbrey equation (eq. (1))[1]:

$$\Delta f_r = -\frac{2{f_q}^2 \Delta m}{A\sqrt{\rho_q \mu_q}} \quad (1)$$

where f_q is the fundamental resonance frequency of quart, A is the piezo-electrically active area of quartz crystal, ρ_q and μ_q are the shear modulus and density of quartz respectively, and Δm is the mass change of the electrode. Note that this Sauerbrey equation is only valid for a rigid and thin deposit on a quartz, and eq. (1) can be simplified as follows:

$$\Delta f = -C_f \Delta m \quad (2)$$

where Δf is the frequency change, and C_f is the sensitivity factor of the quartz crystal. Due to the rigorous correspondence of the oscillation frequency and the mechanical pressure of the quartz crystal, the EQCM has incomparable advantage in weighing tiny mass change with high stability and sensibility, even in the level of 10^{-9} g[2]. Besides, it can also be connected with various electrochemical systems, showing broad adaptability and compatibility[3]. This technique has been widely used in the fields of corrosion[4], catalysis[5, 6], energy storage[7], etc. As an *in situ* testing technique, EQCM is quite suitable for the battery research to build the connection between the mass change and charge transfer of the

Received 12 March 2020; accepted 27 March 2020
① This work was financially supported by Soft Science Research Project of Guangdong Province (No. 2017B030301013)
② Corresponding author. E-mail: panfeng@pkusz.edu.cn
Qin Run-Zhi and Wang Yan contribute equally to this work

electrodes. The high precision of weight measurement makes it possible for some in-depth mechanism research for both cathodes and anodes. For example, the activation pathway of Li-rich Li_2MnO_3 cathodes was clarified[8], and the SEI formation process on the graphite anodes was identified by EQCM[7]. Recently, the metal anodes based on deposition/dissolution mechanisms have attracted tremendous interests in electrochemical energy storage systems. Especially, the Li anode is expected to replace the carbon-based anode for elevated capacity, and Zn anode presents great potential for large-scale energy storage devices owning to the higher capacity[9]. Some advances have been made utilizing EQCM on the metal anodes. Herein, we focus on the application of EQCM in research of metal anodes. The in-depth mechanisms of the electrodeposition/dissolution of Li and Zn anodes are summarized, and an outlook of the further development on the metal anodes is also proposed.

2 PROGRESS OF RESEARCH

2. 1 EQCM study for Li anode

Li anode is highly promising for revolutionizing current rechargeable batteries due to its ultrahigh energy density (3680 $mAh \cdot g^{-1}$). Because of the high reactivity of Li metal, the side reactions between electrolytes, anions and Li metal are almost inevitable. The passivation of electrode surface with the solid electrolyte interphase (SEI) makes it possible to utilize the Li metal anode in the rechargeable Li metal batteries. Thus, the research on SEI becomes a critical component of battery research[10].

EQCM has been extensively applied to investigate the formation of stable SEI by tuning the inorganic salts component in various organic electrolytes. Firstly, the SEI formation and Li under-potential deposition on Au electrode in a $LiAsF_6$-PC electrolyte were investigated by EQCM. The mass change associated with Li striping peak is ~23 $ng \cdot cm^{-2}$, which is larger than mass change obtained from coulometric analysis (~16 $ng \cdot cm^{-2}$), indicating the reduction of solvent and the formation of SEI films accompanied with Li deposition/dissolution process[11]. Naoi et al. studied the SEI formation during deposition/dissolution processes of Li in the electrolytes of $LiClO_4$/$LiSO_3CF_3$/$LiPF_6$ in propylene carbonate (PC) and diethyl carbonate (DEC), respectively[12]. In the $LiPF_6$ system, an increase of mass was observed even during the discharge process for the first three cycles. The less irreversible mass change Δm and smaller resistance change ΔR, which were related to surface roughness, indicated the formation of smooth and uniform LiF-based SEI in $LiPF_6$-containing electrolyte. The obtained SEI was physically stable and self-healing during discharge process, leading to the relatively high columbic efficiency of Li deposition/dissolution in $LiPF_6$ system. On the contrary, the morphology of SEI in $LiClO_4$-containing electrolyte was rough, and the dissolution of Li might cause the destruction of dendritic shape of SEI, making the surface smoother again (Fig. 1a to 1c). Furthermore, Aurbach et al. compared the stability and electrochemical performance of SEI formed during Li deposition/dissolution in $LiAsF_6$/EC-DMC, $LiPF_6$/EC-DME, $LiAsF_6$/EC-THF and $LiAsF_6$/1,3-dioxalone electrolytes, respectively[13]. The actual mass per electron (mpe) value, the columbic efficiency and the mass residual per cycle could be obtained by EQCM calculation, and the results indicated that the $LiAsF_6$/1,3-dioxalone showed best performance among all these systems. Based on EQCM analysis, the $LiAsF_6$/1,3-dioxalone electrolyte shows the best performance among all these systems in the following aspects: (i) the actual mass per electron (mpe) value close to theoretical molar mass of Li, (ii) the high columbic efficiency, and (iii) the little mass residual per cycle. Besides, they also observed that the mpe values calculated by EQCM-CV measurements are smaller than that of the equivalent weight of the surface species, such as $(CH_2OCO_2Li)_2$, indicating the possible dissolution of SEI and/or parts of charge injection into the electrolyte before stable SEI formed[14].

Recently, Smaran et al. have employed EQCM to study the initial SEI formation behavior of the Li anode. The SEI formation process could be identified into three stages: in stage i, the native-SEI formed by potential pre-scan from OCP to 0.35 V; in stage ii, the pre-SEI formed by additional potential cycling between 0.35 and 0 V; and in stage iii, the add-SEI formed during the subsequent Li deposition/deposition process. All these processes can be *in situ* observed and quantificationally measured with EQCM. In LiTFSI and LiFSI-tetraethylene glycol dimethyl ether (TEGDME) systems, the add-SEI was not formed with the presence of pre-SEI and only Li deposition and dissolution were observed based on mpe analysis. These results demonstrated the stabilization effect of pre-SEI for electrode surface (Fig. 1d to 1f)[15]. Besides, Zeng et al. studied the Li metal anode for Li-S batteries with EQCM. With the addition of transition metal cations such as Zn^{2+}, the mass change was larger for the first 5 cycles and less for subsequent cycles compared with electrolyte with no salts. The mass accumulation after 25 cycles was ~1.9 μg with Zn^{2+} additives, as compared to ~3.3 μg without the addition of salts. This could be explained that the Zn^{2+} involved in the SEI formation to create a more uniform and denser passivation layer, leading to the inhibited dendrite growth and electrolyte decomposition[16].

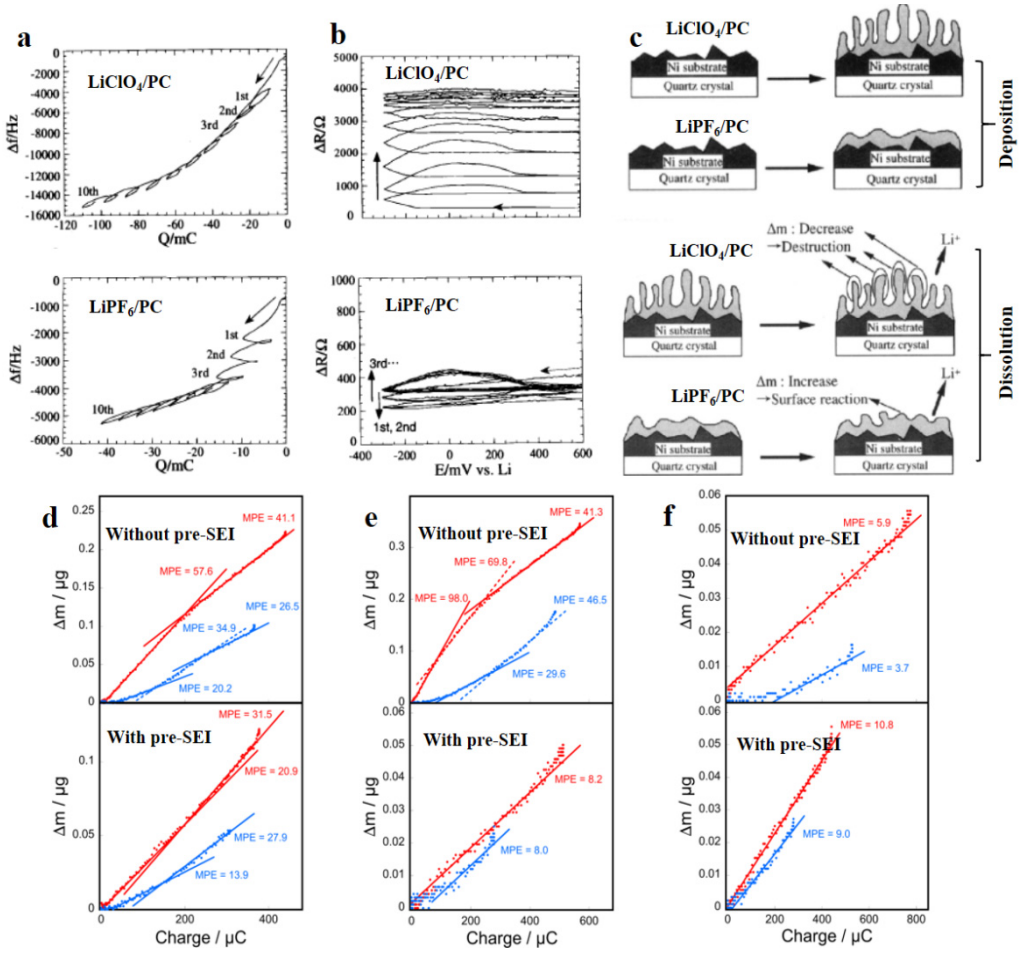

Fig. 1. Effect of inorganic salts on SEI formation for Li anode. (a) Frequency shift *vs.* charge in $LiClO_4$/PC, $LiSO_3CF_3$ and $LiPF_6$/PC; (b) Resistance change *vs.* potential in $LiClO_4$/PC, $LiSO_3CF_3$ and $LiPF_6$/PC; (c) Model of morphology changes of electrodes surface during Li deposition and dissolution[11]. Copyright of Elsevier; (d~f) anodic (blue lines) and cathodic (red lines) charge dependence of Δ*m* value in $LiPF_6$-G4 (d), LiTFSI-G4 (e), LiFSI-G4 (f) with/without pre-SEI[15]. Copyright of ACS

EQCM was also utilized to reveal the Li deposition/dissolution behavior on different metal substrates, such as Pt, Au, Sn, Al, and so on. Park et al. conducted a comparative study of Li deposition/dissolution behavior on Pt, Al, and Hg substrates. The chemical reactions involving elemental Li and the low reduction-oxidation reversibility of Li in the Li-Pt alloys resulted in the low coulombic efficiencies for Li on the Pt substrate (Fig. 2a). The self-discharge rate of Li on the Al substrate was very low (~0.3 mA·cm^{-2}), mainly attributing to the formation of protective films on the surface of Li-Al alloys (Fig. 2b). Besides, the electrochemical reduc- tion of Li on Hg substrates occurring at the least negative potential was mainly due to the amalgam formation (Fig. 2c)[17]. Tavassol et al. also compared the mass change of Li deposition on Au and Sn substrates. The mass change on Sn substrate during deposition was smaller than that of Au substrate, and the SEI is stable for Sn substrate in the initial cycle, while it takes 3 to 4 cycles for Au to be stabilized (Fig. 2d and 2e)[18]. Furtherly, they used the matrix assisted laser desorption ionization time of flight mass spectrometry measurements (MALDI-MS) to monitor the formation of SEI. MALDI-MS on that emersed electrodes showed that long-chain oligomerized species were present on Au surface in both PC and EC/DMC solvents, where the oligomerized species formed in PC solutions showed higher mass ratios (Fig. 2f).

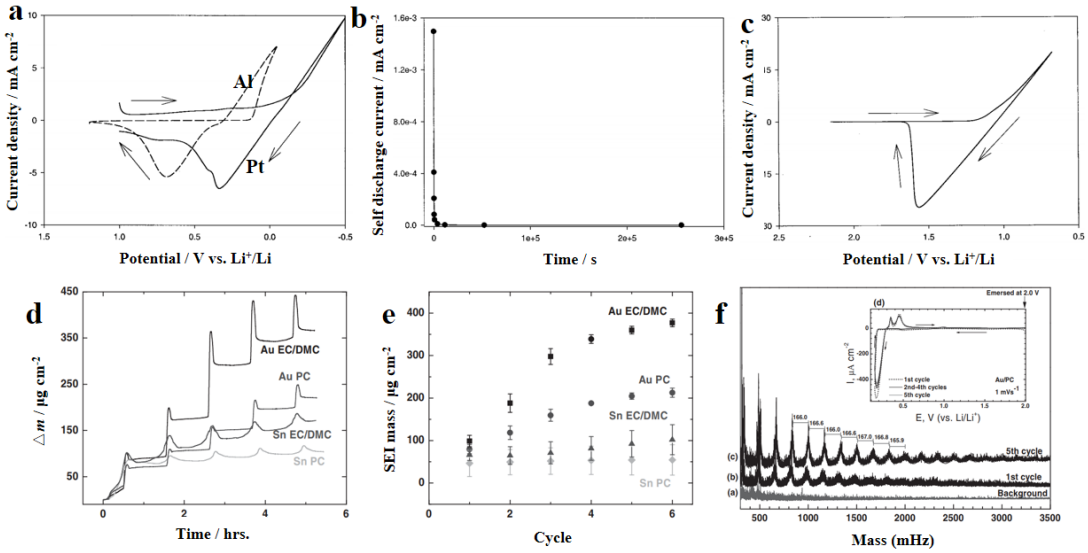

Fig. 2. Deposition/dissolution of Li in different metal substrates. (a) CVs of Al and Pt in LiTFSI-EMSF; (b) Self-discharge rate of Li on Al substrate; (c) CV of Hg electrode in LiTFSI-EMSF[17]. Copyright of Electrochemical Society, Inc. (d) Mass changes as a function of time and (e) Mass of SEI at the end of each cycle for Au and Sn in EC/DMC and PC electrolytes; (f) MALDI-TOF mass spectrometry analysis of textured Au electrodes emersed from 1 M $LiClO_4$/PC after cycling between potentials of 2. 0 to 0.1 V (*vs.* Li/Li$^+$)[18]. Copyright of Electrochemical Society, Inc.

Efforts have also been made to improve the performance of Li anode by organic additives. Naoi et al tried to stabilize the surface film of Li metal with poly(ethylene glycol) dimethyl ether (PEGDME). They made a microelectrode voltammetry (MEV) analysis, which showed that the activation energy ΔG^* increases from 11 to 60 kJ·mol^{-1} as the molecular weight (Mw) was increased from 90 to 400 (Fig. 3a). The enlarged ΔG^* indicated that Li ions were preferentially coordinated with ethylene oxide (EO) chains, and were incorporated into the helix structures of EO chains when PEGDME with repeated EO units (Mw about 180~2000) was added to the electrolytic solution. The addition of PEGDME promoted the formation of improved SEI, thus facilitating the uniform

diffusion of Li^+ in SEI and the subsequent deposition of Li (Fig. 3b). Based on EQCM measurement, the addition of PEGDME decreased the inactive mass of Li during deposition-dissolution cycles on Ni electrode (Fig. 3c and 3d). The least extent of inactivation of Li was achieved when the molecular weight of PEGDME was ~400[19]. △m / μg cm-2

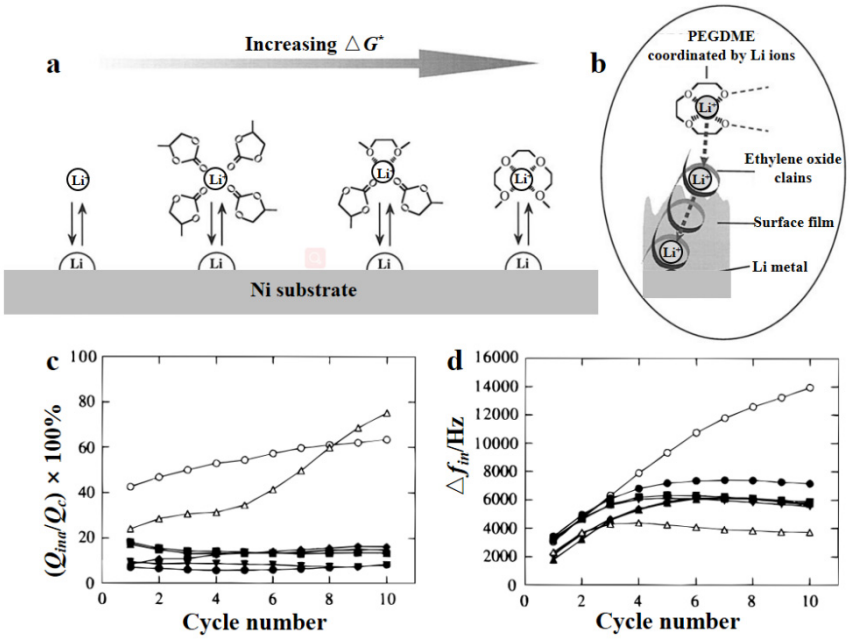

Fig. 3. Modification of the Li metal surface by nonionic polyether surfactants. (a) Postulated model of the electron transfer for Li/Li(I) couples under various solvated conditions; (b) Postulated model for Li ion diffusion in the PEGDME-added systems; (c) Q_{ina}/Q_c and (b) D_{firr} *vs.* cycle number plots for the deposition and dissolution processes of Li on Ni obtained from CV/QCM. (○) $LiClO_4$/PC, (△) $LiClO_4$/PC + Mw 90, (◆) $LiClO_4$/PC + Mw 180, (▼) $LiClO_4$/PC + Mw 250, (●) LiClO4/PC + Mw 400, (■) $LiClO_4$/PC + Mw 1000, and (▲) $LiClO_4$/PC + Mw 2000[19]. Copyright of Electrochemical Society, Inc.

EQCM was also employed to study the complicated electrolyte systems. Serizawa et al. and Matsumoto et al. have applied EQCM in molten electrolyte and ionic liquids, respectively. Due to the influence of concentration on viscosity of the electrolyte and the correlation between viscosity and frequency of EQCM, the mass change deviates from the linear relationship of Sauerbrey eq. (1). Therefore, the impedance technique EQCM was employed to simultaneously monitor the resonance resistance R_{res}, which could be related to the product of viscosity η_L and density ρ_L of media in contact with the electrode. The change of $\eta_L\rho_L$ value reflected the concentration change near the electrode during Li deposition and dissolution. In the potentiostatic experiment, a sharp increase in $\eta_L\rho_L$ during Li dissolution was observed, which caused a decrease in anodic peak and affected the diffusion of Li^+ from electrode surface to bulk phase. The $\eta_L\rho_L$ value decreased after Li dissolution, which could be attributed to the relaxation of Li^+ concentration near the electrode[20]. In ionic liquids, however, very complicated results were obtained by EQCM due to complex viscosity change in the systems. More work needs to be done in the future to understand the Li deposition and dissolution in ionic liquids[21].

2. 2 EQCM study for Zn anode

Due to the merits of high theoretical capacity (820 $mAh{\cdot}g^{-1}$), low electrochemical potential (−0.76 V *vs.* SHE), and high natural abundance, the Zn anodes have been extensively studied in various battery systems, including alkaline primary Zn batteries, rechargeable Zn ion batteries, Zn-air batteries, etc[22, 23]. Most of these battery systems employ aqueous electrolytes, showing lower toxicity and higher safety than that of the non-aqueous electrolyte systems of

the Li ion batteries. Therefore, the Zn-based batteries have been considered as a more affordable option for price-conscious scopes, e.g. the large-scale energy storage applications.

EQCM was utilized to study the 2-electron occupied deposition/solution reactions of Zn anodes in aqueous electrolyte. Agrisuela et al. conducted a series of EQCM experiments in $ZnSO_4$ solution[24]. The electro-deposition voltammetry diagram together with the mass/electrical charge ratio at specific potential (F(*dm*/*dQ*) function) is shown in Fig. 4a. The average mass/electrical charge ratio is ~34 $g \cdot mol^{-1}$, which is close to the theoretic value of the divalent Zn reduction reaction (−32.7 $g \cdot mol^{-1}$):

$$Zn^{2+} + 2e \rightarrow Zn \quad (3)$$

However, this value varied in each zone during the potential scan. This indicated that the reduction of Zn^{2+} might take place via two consecutive single-electron transfer steps:

$$Zn^{2+} + e \rightarrow Zn^{+} \quad (4)$$

$$Zn^{+} + e \rightarrow Zn \quad (5)$$

where one showed 0 $g \cdot mol^{-1}$ for a homogeneous process, and another showed −65.4 $g \cdot mol^{-1}$ for a heterogeneous process. When the scan rate increased, the F(*dm*/*dQ*) function in zone 1 (the initial stage of the potential scan in Fig. 4b) tended to be zero, which indicated the value of the F(*dm*/*dQ*) function for the first transfer step is 0 $g \cdot mol^{-1}$. Besides, the formed Zn^{+} ions might neither absorb on the electrode, nor diffuse into the bulk electrolyte, but stay in a special layer between them. Only in this way, the mass/electrical charge ratio of the global process and each detailed zone could make sense. Upon deposition, the two reaction steps overlapped during the voltammetry measurement. Additionally, the motional resistance R_m was calculated and provided another evidence in Fig. 4c. In the diagram of current-motional resistance response, the R_m remained constant in zone 1, indicating that the faradaic processes of the first step did not change the rigidity of the electrode, which was coincident with the mass change results. Therefore, the author proposed the Zn deposition mechanism in Fig. 4d. The Zn^{2+} ions were first reduced into the intermediate Zn^{+} ions in a viscoelastic layer, then the Zn^{+} ions were deposited on the electrode. Likewise, the electro-dissolution of Zn metal is also reported to take two steps, and the intermediates Zn^{+} ions are also demonstrated in EQCM studies[25]. In this way, the EQCM shows unique and precise identification of the reaction path in the multi-electron reactions.

As an amphoteric metal, Zn could get corroded in the aqueous electrolyte, which leads to the self-discharge and capacity loss in battery systems. The impedance and polarization techniques are widely used to observe the corrosion[27]. However, only static information could be acquired via indirect calculations. Wang et al. employed the EQCM to monitor the corrosion of Zn anode in acidic solutions[4]. The frequency of the quartz crystal under open-circuit potential increased linearly with time. Following Eq. 5, the slop of the frequency curve made it possible to evaluate the real-time corrosion rate, indicating a continuous and homogenous corrosion in Fig. 4e:

$$V = \frac{\Delta M}{\Delta t \cdot A} = -\frac{\Delta f}{\Delta t \cdot S} \quad (6)$$

where V is the corrosion rate, Δt the experiment time, A the surface area of electrode, and S a constant factor related to the cell. Interestingly, similar experiment was conducted by Hwang et al. in alkaline solutions[26], but the results are quite different (Fig. 4f). The frequency increased initially then reached plateau after 500 s, which was attributed to the block of the electrode surface by corrosion products. The electrode then got passivated after the initial corrosion. As mentioned above, this transformation procedure could not be identified by the traditional methods. The passivation of Zn anodes in alkaline electrolyte was further studied by Wittman and co-workers[28]. The EQCM data provided key assistance on the determination of the passivation, which was caused by electrochemical etching, leading to a build-up of solid ZnO and $Zn(OH)_2$ layer. It is clear that the corrosion mechanism of Zn anodes varies in different electrolytes, and EQCM exhibits advantages in monitoring the real-time and dynamic corrosion/pas- sivation process.

Generally, the short-circuit failure of the Zn anode in aqueous batteries often results from the severe

dendrite issues[29, 30]. Using additives is an effective way to suppress the dendrite and to achieve the uniform surface deposition. Miyazaki et al. studied the influence of cetyltrimethylammonium bromide (CTAB) on Zn electrodeposition[31]. As shown in the CV and EQCM diagrams in Fig. 5a, the reduction potentials shifted negatively both for the current and frequency after adding CTAB. Besides, small spherical deposits rather than the sharp dendrite were observed for the SEM morphology of Zn anode after cycling (Fig. 5b, 5c). Therefore, the author supposed the adsorption of CTAB on the electrodes effectively decelerates the growth of Zn deposition and hinders the dendrite formation.

The adsorption of additives was confirmed by Ballesteros et al. via a negative potential scan in a Zn^{2+}-free electrolyte[32]. The EQCM results showed the partial desorption/adsorption of polyethylene glycol (PEG) in the interval of −1.3 to −1.1 V (*vs.* SCE), and a substantial desorption in the interval −1.4 to −1.7 V (*vs.* SCE). It was proposed that the adsorption of PEG blocked some active sites on the electrode, then the reduction of Zn^{2+} ions occurred only at the rest of the active sites. The mechanism was further studied and vividly depicted by Mitha et al., as shown in Fig. 5d[33]. The 2D diffusion of Zn^{2+}

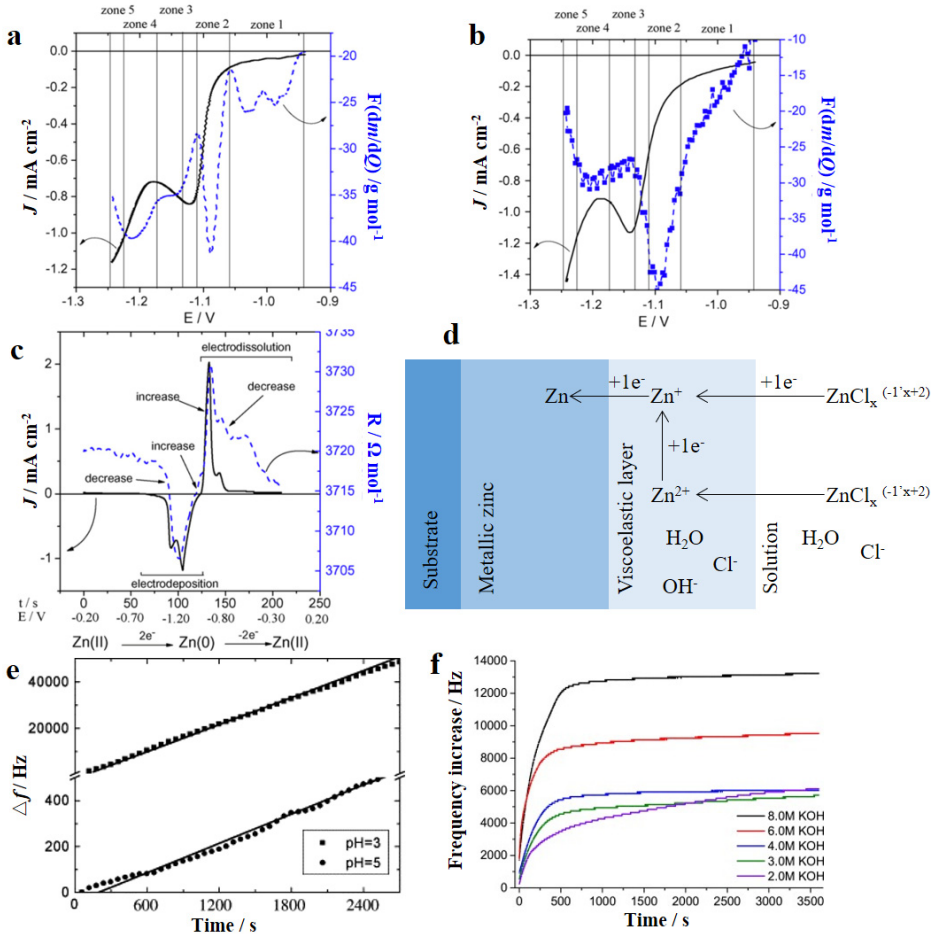

Fig. 4. (a) F(*dm*/*dQ*) function during the cathodic scan in electrolyte of $ZnSO_4$ 10 mM, Na_2SO_4 1.32 M, H_3BO_3 0.32 M and NH_4Cl 0.26 M, pH 4.80, scan rate 10 mV/s; (b) F(*dm*/*dQ*) function during the cathodic scan in electrolyte of $ZnSO_4$ 10 mM, Na_2SO_4 1.32 M, H_3BO_3 0.32 M and NH_4Cl 0.26 M, pH 4.80, scan rate 80 mV/s; (c) Current-motional resistance response during the voltammetric scan between −0.20 and −1.25 V; (d) Schematic representation of mechanism proposed for the Zn electrodeposition process[24]; (e) Typical frequency shift-time curves measured of Zn electrode in dilute H_2SO_4 aqueous solutions[4]; (f) Typical frequency-time curves of Zn electrode in KOH solutions[26]. Copyright of Elsevier.

ions was effectively constrained by the physical barriers of the adsorbed PEG polymers on the electrode surface. Thus, the Zn^{2+} ions were forced to deposit in a very limited area nearby where the initial adsorption occurred, leading to more nucleation sites of Zn deposition. Therefore, the addition of PEG resulted in a 2D instantaneous nucleation rather than the 3D diffusion-controlled nucleation process, making a smoother and more compact Zn surface.

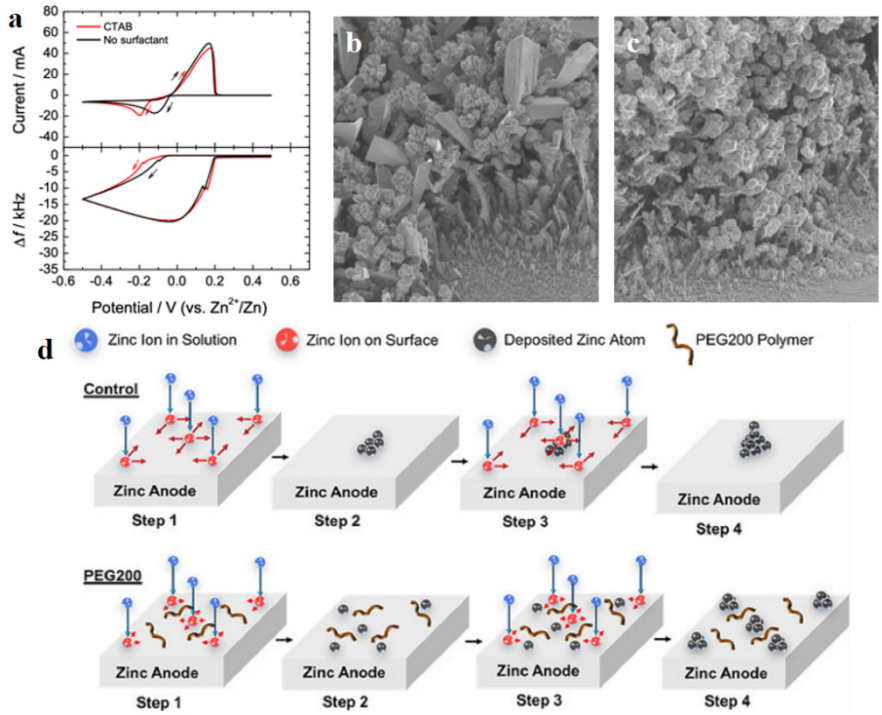

Fig. 5. Effect of additives on Zn deposition. (a) Cyclic voltammograms and frequency-potential curves with and without CTAB in the first cycle; SEM images of Zn deposits formed by applying current densities of 20 mA·cm^{-2} for 1 h with (b) and without CTAB (c)[31], (d) Schematics of the step-by-step Zn reduction and deposition processes in control and PEG200 electrolytes under negative potential on the Zn electrode[33]. Copyright of Wiley.

In the same way, the influence of other additives has also been discussed using EQCM, including boric acid[34], benzylideneacetone[35], thiourea, gelatin[36], nicotinic acid, benzoquinone[37], etc. The species and concentrations of the additives were optimized in different electrolytes. However, the Zn deposition gets different morphologies with different additives, which may indicate the crystal orientation of Zn was affected by the selected molecules. The function of additives in microscale crystallography needs further study.

3 CONCLUSION AND OUTLOOK

With the ability of *in situ* weighing tiny mass changes, EQCM has been well known as a powerful tool for the research on the electrochemical process of metal anodes in battery systems, especially for quantitative mass measurement and reaction path identification. For Li anodes, the Li deposition and dissolution are unavoidably accompanied with SEI formation. The morphology, reversibility and stability of SEI have been comparatively studied in a large variety of solvents, salts and additives. This *in situ* characterization is helpful for better understanding the protection of Li metal anode by SEI. For Zn anodes, the intermediates of Zn^{+} ions were found in a viscoelastic layer, and the corresponding 2-steps model of dissolution/deposition has been proposed. The effect of various additives for dendrite suppression was estimated and illustrated.

Although great progress has been achieved, the EQCM is supposed to service more on in-depth electrochemical mechanism. First, the collapse of Li dendrite structure is considered as one of the reasons of irreversible mass change during cycles. However, EQCM can't determine the influence of this effect solely, and the combination of other analytical techniques is necessary. With the development of new methods such as 3D composite electrode, more improvements are needed for EQCM to adapt to these new systems. Furthermore, since the Zn^+ ions play an important role in deposition, they might make an impact on the dendrite formation. However, this issue was less discussed in the literature, and such mechanism remains unrevealed. Thus, the connection between the dendrite and the ions, as well as the viscoelastic layer, should share more attention. In the end, the additives show strong control effect on the Zn morphology, but the simple adsorption model seems not suitable for all kinds of additives. More work needs to be conducted to understand the detailed principle of each additive.

REFERENCES

(1) Sauerbrey, G. Verwendung von schwingquarzen zur wägung dünner schichten und zur mikrowägung. *Z. Physik.* **1959**, 155, 206–222.

(2) Kanazawa, K. K.; Gordon, J. G. The oscillation frequency of a quartz resonator in contact with liquid. *Anal. Chim. Acta* **1985**, 175, 99–105.

(3) Grey, C. P.; Tarascon, J. M. Sustainability and *in situ* monitoring in battery development. *Nat. Mater.* **2017**, 16, 45–56.

(4) Wang, D. H.; Tang, X.; Qiu, Y. Y.; Gan, F. X.; Chen, G. Z. A study of the film formation kinetics on zinc in different acidic corrosion inhibitor solutions by quartz crystal microbalance. *Corros. Sci.* **2005**, 47, 2157–2172.

(5) Frydendal, R.; Paoli, E. A.; Knudsen, B. P.; Wickman, B.; Malacrida, P.; Stephens, I. E. L.; Chorkendorff, I. Benchmarking the stability of oxygen evolution reaction catalysts: the importance of monitoring·mass losses. *Chemelectrochem* **2014**, 1, 2075–2081.

(6) Zhao, Q.; Yang, J.; Liu, M.; Wang, R.; Zhang, G.; Wang, H.; Tang, H.; Liu, C.; Mei, Z.; Chen, H.; Pan, F. Tuning electronic push/pull of Ni-based hydroxides to enhance hydrogen and oxygen evolution reactions for water splitting. *ACS Catal.* **2018**, 8, 5621–5629.

(7) Liu, T.; Lin, L.; Bi, X.; Tian, L.; Yang, K.; Liu, J.; Li, M.; Chen, Z.; Lu, J.; Amine, K.; Xu, K.; Pan, F. *In situ* quantification of interphasial chemistry in Li-ion battery. *Nat. Nanotechnol.* **2019**, 14, 50–56.

(8) Yin, Z. W.; Peng, X. X.; Li, J. T.; Shen, C. H.; Deng, Y. P.; Wu, Z. G.; Zhang, T.; Zhang, Q. B.; Mo, Y. X.; Wang, K.; Huang, L.; Zheng, H.; Sun, S. G. Revealing of the activation pathway and cathode electrolyte interphase evolution of Li-rich $0.5Li_2MnO_3{\cdot}0.5LiNi_{0.3}Co_{0.3}Mn_{0.4}O_2$ cathode by *in situ* electrochemical quartz crystal microbalance. *ACS Appl. Mater. Interfaces* **2019**, 11, 16214–16222.

(9) Liu, M.; Zhao, Q.; Liu, H.; Yang, J.; Chen, X.; Yang, L.; Cui, Y.; Huang, W.; Zhao, W.; Song, A.; Wang, Y.; Ding, S.; Song, Y.; Qian, G.; Chen, H.; Pan, F. Tuning phase evolution of β-MnO_2 during microwave hydrothermal synthesis for high-performance aqueous Zn ion battery. *Nano Energy* **2019**, 64, 103942.

(10) Lin, D.; Liu, Y.; Cui, Y. Reviving the lithium metal anode for high-energy batteries. *Nat. Nanotechnol.* **2017**, 12, 194–206.

(11) Mo, Y. B.; Gofer, Y.; Hwang, E. J.; Wang, Z. H.; Scherson, D. A. Simultaneous microgravimetric and optical reflectivity studies of lithium underpotential deposition on Au(111) from propylene carbonate electrolytes. *J. Electroanal. Chem.* **1996**, 409, 87–93.

(12) Naoi, K.; Mori, M.; Shinagawa, Y. Study of deposition and dissolution processes of lithium in carbonate-based solutions by means of the quartz-crystal microbalance. *J. Electrochem. Soc.* **1996**, 143, 2517–2522.

(13) Aurbach, D.; Moshkovich, M. A study of lithium deposition-dissolution processes in a few selected electrolyte solutions by electrochemical quartz crystal microbalance. *J. Electrochem. Soc.* **1998**, 145, 2629–2639.

(14) Aurbach, D.; Moshkovich, M.; Cohen, Y.; Schechter, A. The study of surface film formation on noble-metal electrodes in alkyl carbonates/Li salt solutions, using simultaneous in situ AFM, EQCM, FTIR, and EIS. *Langmuir*. **1999**, 15, 2947–2960.

(15) Smaran, K. S.; Shibata, S.; Omachi, A.; Ohama, A.; Tomizawa, E.; Kondo, T. Anion-dependent potential precycling effects on lithium deposition/dissolution reaction studied by an electrochemical quartz crystal microbalance. *J. Phys. Chem. Lett.* **2017**, 8, 5203–5208.

(16) Zeng, W.; Cheng, M. M. C.; Ng, S. K. Y. Effects of transition metal cation additives on the passivation of lithium metal anode in Li-S batteries. *Electrochim. Acta* **2019,** 319, 511–517.

(17) Park, S. H.; Winnick, J.; Kohl, P. A. Investigation of the lithium couple on Pt, Al, and Hg electrodes in lithium imide-ethyl methyl sulfone. *J. Electrochem. Soc*. **2002**, 149, A1196–A1200.

(18) Tavassol, H.; Buthker, J. W.; Ferguson, G. A.; Curtiss, L. A.; Gewirth, A. A. Solvent oligomerization during SEI formation on model systems for Li-ion battery anodes. *J. Electrochem. Soc.* **2012,** 159, A730−A738.

(19) Naoi, K.; Mori, M.; Naruoka, Y.; Lamanna, W. M.; Atanasoski, R. The surface film formed on a lithium metal electrode in a new imide electrolyte, lithium bis(perfluoroethylsulfonylimide) [$LiN(C_2F_5SO_2)_2$]. *J. Electrochem. Soc.* **1999,** 146, 462−469.

(20) Serizawa, N.; Seki, S.; Takei, K.; Miyashiro, H.; Yoshida, K.; Ueno, K.; Tachikawa, N.; Dokko, K.; Katayama, Y.; Watanabe, M.; Miura, T. EQCM measurement of deposition and dissolution of lithium in glyme-Li salt molten complex. *J. Electrochem. Soc.* **2013,** 160, A1529−A1533.

(21) Matsumoto, H.; Tsuzuki, S.; Kubota, K. *Lithium Redox in Imidazolium Ionic Liquids Composed of Five-membered Cyclic Amide in 17th International Meeting on Lithium Batteries*. Fergus, J. W. Editor **2014**, 223−230.

(22) Jia, H.; Wang, Z.; Tawiah, B.; Wang, Y.; Chan, C. Y.; Fei, B.; Pan, F. Recent advances in zinc anodes for high-performance aqueous Zn-ion batteries. *Nano Energy* **2020**, 70, 104523.

(23) Zhao, Q.; Chen, X.; Wang, Z.; Yang, L.; Qin, R.; Yang, J.; Song, Y.; Ding, S.; Weng, M.; Huang, W.; Liu, J.; Zhao, W.; Qian, G.; Yang, K.; Cui, Y.; Chen, H.; Pan, F. Unravelling H^+/Zn^{2+} synergistic intercalation in a novel phase of manganese oxide for high-performance aqueous rechargeable battery. *Small.* **2019**, 15, 1904545.

(24) Agrisuelas, J.; Garcia-Jareno, J. J.; Gimenez-Romero, D.; Vicente, F. An electromechanical perspective on the metal/solution interfacial region during the metallic zinc electrodeposition. *Electrochim. Acta* **2009**, 54, 6046−6052.

(25) Gimenez-Romero, D.; Garcia-Jareno, J. J.; Vicente, F. EQCM and EIS studies of $Zn_{aq}^{2+} + 2e^- \rightleftarrows Zn^0$ electrochemical reaction in moderated acid medium. *J. Electroanal. Chem.* **2003**, 558, 25−33.

(26) Hwang, B.; Oh, E. S.; Kim, K. Observation of electrochemical reactions at Zn electrodes in Zn-air secondary batteries. *Electrochim. Acta* **2016**, 216, 484−489.

(27) Cai, Z.; Ou, Y.; Wang, J.; Xiao, R.; Fu, L.; Yuan, Z.; Zhan, R.; Sun, Y. Chemically resistant Cu–Zn/Zn composite anode for long cycling aqueous batteries. *Energy Storage Materials* **2020**, 27, 205−211.

(28) Wittman, R. M.; Sacci, R. L.; Zawodzinski, T. A. Elucidating·mechanisms of oxide growth and surface passivation on zinc thin film electrodes in alkaline solutions using the electrochemical quartz crystal microbalance. *J. Power Sources* **2019**, 438, 227034.

(29) Liu, M.; Yang, L.; Liu, H.; Amine, A.; Zhao, Q.; Song, Y.; Yang, J.; Wang, K.; Pan, F. Artificial solid-electrolyte interface facilitating dendrite-free zinc metal anodes via nanowetting effect. *ACS Appl. Mater. Interfaces* **2019**, 11, 32046−32051.

(30) Wang, Z.; Hu, J.; Han, L.; Wang, Z.; Wang, H.; Zhao, Q.; Liu, J.; Pan, F. A MOF-based single-ion Zn^{2+} solid electrolyte leading to dendrite-free rechargeable Zn batteries. *Nano Energy* **2019**, 56, 92−99.

(31) Miyazaki, K.; Nakata, A.; Lee, Y. S.; Fukutsuka, T.; Abe, T. Influence of surfactants as additives to electrolyte solutions on zinc electrodeposition and potential oscillation behavior. *J. Appl. Electrochem.* **2016**, 46, 1067−1073.

(32) Ballesteros, J. C.; Diaz-Arista, P.; Meas, Y.; Ortega, R.; Trejo, G. Zinc electrodeposition in the presence of polyethylene glycol 20000. *Electrochim. Acta* **2007**, 52, 3686−3696.

(33) Mitha, A.; Yazdi, A. Z.; Ahmed, M.; Chen, P. Surface adsorption of polyethylene glycol to suppress dendrite formation on zinc anodes in rechargeable aqueous batteries. *Chemelectrochem.* **2018**, 5, 2409−2418.

(34) Trejo, G.; Ruiz, H.; Borges, R. O.; Meas, Y. Influence of polyethoxylated additives on zinc electrodeposition from acidic solutions. *J. Appl. Electrochem.* **2001**, 31, 685−692.

(35) Moron, L. E.; Mendez, A.; Ballesteros, J. C.; Antano-Lopez, R.; Orozco, G.; Meas, Y.; Ortega-Borges, R.; Trejo, G. Zn electrodeposition from an acidic chloride bath containing polyethyleneglycol (Mw 200) and benzylideneacetone as additives. *J. Electrochem. Soc*. **2011**, 158, D435−D444.

(36) Song, K. D.; Kim, K. B.; Han, S. H.; Lee, H. Effect of additives on hydrogen evolution and absorption during Zn electrodeposition investigated by EQCM. *Electrochem. Solid St.* **2004**, 7, C20−C24.

(37) Alesary, H. F.; Cihangir, S.; Ballantyne, A. D.; Harris, R. C.; Weston, D. P.; Abbott, A. P.; Ryder, K. S. Influence of additives on the electrodeposition of zinc from a deep eutectic solvent. *Electrochim. Acta* **2019**, 304, 118−130.